Published in final edited form as:

Nat Struct Mol Biol. 2018 February ; 25(2): 163–169. doi:10.1038/s41594-018-0022-z.

Solution Structure and Elevator Mechanism of the Membrane Electron Transporter CcdA

Yunpeng Zhou[1,*] and **John H. Bushweller**[1,2,*]

[1]Department of Molecular Physiology and Biological Physics, University of Virginia, Charlottesville, Virginia, USA

[2]Department of Chemistry, University of Virginia, Charlottesville, Virginia, USA

Abstract

Membrane oxidoredutase CcdA plays a central role in supplying reducing equivalents from the bacterial cytoplasm to the envelope. It transports electrons across the membrane using a single pair of cysteines by a mechanism which has not been elucidated. Here we report an NMR structure of the *Thermus thermophilus* CcdA (TtCcdA) in an oxidized and outward-facing state. CcdA consists of two inverted structural repeats of three transmembrane helices (2 × 3-TM). We computationally modeled and experimentally validated an inward-facing state, which suggests that CcdA uses an elevator-type movement to shuttle the reactive cysteines across the membrane. CcdA belongs to the LysE superfamily. Its structure may be relevant to other LysE clan transporters. Structure comparisons of CcdA, semiSWEET, Pnu, and major facilitator superfamily (MFS) transporters provide insights about membrane transporter architecture and mechanism.

Introduction

Cells regulate redox homeostasis by compartments. The bacterial cytoplasm is reducing to prevent oxidative damage whereas the periplasm is oxidizing to promote oxidative protein folding. Crucial reducing pathways exist in the periplasm which rely on external reducing sources. The membrane electron transporter CcdA (as well as the TM domain of DsbD and ScsB) introduces reducing equivalents from the cytoplasm to the periplasm[1–6]. This is critical for various cellular functions such as cytochrome c biogenesis, lithotrophic sulfur oxidation, oxidative protein folding, and defense against oxidative damage[7–9]. In addition to bacteria and archeae, CcdA homologs have been found on the thylakoid membrane of chloroplasts to promote cytochrome c maturation, a process essential for photosynthesis[10].

CcdA has six transmembrane helices arranged in two sequence repeats, TM 1–3 and TM 4–6 (Supplementary Fig. 1a)[11]. A pair of redox active cysteines is located in two conserved

*Correspondence to: yz8w@virginia.edu, jhb4v@virginia.edu.

Author Contribution Y.Z. and J.H.B. designed the research; Y.Z. performed the experiments and analyzed the data; Y.Z. and J.H.B. wrote the manuscript.

Competing financial interests

The authors declare no competing financial interests.

PCxxP motifs on TM1 and TM4[12,13]. The reducing equivalents are transferred through a cascade of thiol:disulfide exchange reactions from the cytoplasmic general reductant thioredoxin (Trx) to CcdA, across the membrane, then to various periplasmic redox-active proteins (Fig. 1a)[1–4]. The periplasmic substrates use a Trx-fold domain to react with CcdA[7]. Thus CcdA conducts similar redox reactions on both sides of the membrane. Cysteine scanning mutagenesis studies probing the solvent accessibility of *E. coli* DsbD (EcDsbD), a CcdA homolog, suggests it has an inverted pseudosymmetry[14,15], which is consistent with the dual accessibilities of the reactive cysteines by the Trx substrates from both sides of the membrane.

CcdA is unique among membrane electron transporters. It uses a single pair of cysteines relaying electrons across the cytoplasmic membrane without the help of cofactors[16]. To understand the molecular basis of its mechanism, we solved the structure of TtCcdA using solution NMR spectroscopy. The structure represents an oxidized and outward-facing state. We have also computationally modeled and experimentally validated an inward-facing state of oxidized TtCcdA which suggests that the active cysteine pair is shuttled across the membrane in an elevator-type movement.

Results

Sample conditions and NMR structure determination

We have screened multiple CcdA proteins from bacteria and archaea for the feasibility of solution NMR studies. Oxidized TtCcdA was stable, mono-disperse, and showed promising initial NMR spectra (Fig. 1b and Supplementary Fig. 1b). An E35A mutation was introduced to suppress truncation during heterogeneous expression. The protein was partially oxidized during expression and became fully oxidized after purification. Purified TtCcdA is redox active with its native Trx substrate (Supplementary Fig. 1c). The structure represents an oxidized conformation in which the redox active disulfide bond is formed. Reduced TtCcdA shows conformational heterogeneity and increased dynamics so a structure determination was not feasible (Fig. 1c). For oxidized TtCcdA, 86% of the backbone resonances and 58% of the side chain β carbon resonances have been assigned. The long-range restraints used to determine the global fold of TtCcdA are derived from eight paramagnetic relaxation enhancement (PRE) samples and residual dipolar couplings (RDC) measured in two alignment conditions (Table 1 and Supplementary Fig. 2a–d)[17–19]. These restraints were measured using sensitive 2D ^{15}N-^{1}H TROSY based experiments and rely on the readily obtained protein backbone amide resonance assignments[19,20].

The structure of oxidized TtCcdA was validated in two ways. First, we calculated a series of ensemble structures using partial long-range RDC and PRE restraints (Supplementary Fig. 2e). These structures could be examined using the withheld RDC restraints. The low Q_{free} factors are indicative of the quality of these structures. The reported structure, which is calculated with all restraints, is very similar to these partially restrained structures. Second, solvent accessibility data were obtained using the water-soluble paramagnetic reagent Gd-DTPA (Supplementary Fig. 3a–b). Residues accessible to the solvent and the paramagnetic reagent exhibit marked NMR signal intensity reduction. These residues are in the periplasmic and cytoplasmic loops. Residues with relatively small signal reduction are in the

central regions of the TM helices. The solvent accessibility data is in good agreement with the structure of TtCcdA.

Structure of oxidized TtCcdA is in an outward-facing state

The most prominent structural feature of TtCcdA is the symmetry of the 3-TM repeats (Fig. 2a–b). For convenience of discussion, we name the three helices of the 3-TM repeats A, B, and C-helix. The A-helix is long and bends ~ 60° at the central PCxxP motif. The B and C-helices together form a "U" shape. A characteristic bend in the C-terminal one third of the B-helix forms the bottom of the "U". The two 3-TM repeats are antiparallel to one another. Each inserts its A-helix into the "U" of the opposite one. A-helices TM1 and TM4 are central transport helices and are connected by the active site disulfide bond. Outside, C-helices TM3 and TM6 pack tightly against each other via a pair of conserved Gx_6G motifs (Supplementary Fig. 3c). B-helices TM2 and TM5 form similar packing. The two inverted "U"s stack together forming an "O" scaffold domain. Based on the membrane orientation prediction using the PPM server[21], the "O" scaffold is highly tilted with its long axis passing through residues 69 and 176 forming a 38° angle with the membrane norm, which results in a resemblance of the interior portion of the "O" to a channel. The loops connecting the two central A-helices and the "O" scaffold (L1, L3, and L4) are flexible (Supplementary Fig. 3d). The overall architecture of TtCcdA could be described as two kinked transport helices inserted into an "O" scaffold channel with flexible loops connecting them (Fig. 2c).

The NMR structure of oxidized TtCcdA represents an outward-facing state. This results from TM1 and TM4 adopting different orientations relative to the "O" scaffold (Fig. 2b). Viewed from the periplasmic side, the disulfide bond is at the bottom of a shallow pocket surrounded by the N-terminus of TM3, TM4b, the C-terminus of TM6, and H1 (Fig. 2c). From the cytoplasmic side, TM1b and TM4a block access to the disulfide bond. The N_{out}-C_{out} membrane topology is inferred using the "positive inside" rule and is consistent with previous studies (Supplementary Fig. 3e)[10,22].

Comparison to *Archaeoglobus fulgidus* CcdA (AfCcdA)

We have compared our structure with the published NMR structure of an AfCcdA mutant which mimics the reduced state of the protein[23]. The two proteins show significant sequence homology (29% identity, 60% similarity) but bear no structural resemblance (Fig. 2a–c versus Supplementary Fig. 4a). There are several lines of evidence supporting the structure of TtCcdA as consistent with previous bioinformatics and biochemical analysis of CcdA transporters. First, the internal sequence repeats of CcdA suggests they encode similar structural units[11]. The two repeats of TtCcdA encode symmetry related TM1–3 and TM4–6. The N-terminal repeat of AfCcdA encodes TM1–3 and the C-terminal repeat encodes two consecutive horizontal helices (h and h′) and TM5–6. The two parts of AfCcdA do not display discernible structural similarity. Second, bioinformatics analysis and membrane topology assays show a consensus that the two conserved PCxxP motifs are located in TM1 and TM4[10,14,22], which is in agreement with the structure of TtCcdA. In contrast, the first PCxxP motif of AfCcdA is in the cytoplasmic loop between TM1 and TM2 and the second PCxxP motif is between h and h′. Third, multiple sequence alignment shows the residues connecting the two repeats are highly variable and hydrophilic (Supplementary Fig. 4c–d).

This region encodes a cytoplasmic loop (L3) in TtCcdA and a TM helix (TM4) in AfCcdA. Fourth, the inverted symmetry solvent accessibility profile of EcDsbD matches the structure of TtCcdA but not AfCcdA (Supplementary Fig. 4b and see next section)[14,15]. In addition, the global fold of TtCcdA was determined using redundant and self-consistent long-range PRE and RDC restraints (on average 7 per residue) while that of AfCcdA used sparse and iteratively assigned long-range NOEs (on average 0.5 per residue) (Supplementary Note). The structure of TtCcdA is validated using RDCs and the low Q_{free} factors are indicative of the quality of the structure (Supplementary Fig. 2e). The structure of AfCcdA was qualitatively validated using PRE restraints. Some restraints depart from the structural model and the difference was ascribed to potential conformational exchange or transient aggregation of AfCcdA.

An inward-facing model of oxidized TtCcdA

Oxidized TtCcdA is in an outward-facing state. In order for the protein to be reduced by cytoplasmic Trx, it needs to switch to an inward-facing state in which the disulfide bond is exposed to the cytoplasm. Imperfect structural symmetry of sequence repeats implies underlying conformational flexibility. An established “repeat-swap homology modeling” approach switches the conformations of the repeats and predicts the inward-facing state from an outward-facing structure or vice versa[24]. Using this approach, we swapped the conformations of TM1–3 and TM4–6 of TtCcdA, which effectively switches the orientations of TM1 and TM4 relative to the “O” scaffold (Fig. 3a and Supplementary Fig. 5a–b). In the repeat-swap model, the disulfide bond is located at the bottom of a shallow cytoplasmic pocket composed of the N-terminus of TM6, TM1b, the C-terminus of TM3, and the flexible loop L3. TM1a and TM4b seal the disulfide bond off from the periplasm. This model represents a putative inward-facing state of oxidized TtCcdA.

We validated the model using a cysteine cross-linking experiment[25]. A scaffold residue (F45) and a transport helix residue (A113) are distant (13 Å Cα-Cα) in the outward-facing structure but close (6 Å Cα-Cα) in the inward-facing model. We constructed a F45C/A113C mutant. The purified mutant has its native disulfide bond formed as its ^{15}N-^{1}H HSQC NMR spectrum resembles that of the oxidized wild-type protein (Supplementary Fig. 6a). The two introduced cysteines are free to be alkylated (Fig. 3b lane 3). Preincubation of the mutant with equimolar $HgCl_2$ prevents the two free cysteines from alkylation, indicating a “-S-Hg-S-” bridge is formed between F45C and A113C (Fig. 3b lane 5). This bridge is intramolecular because otherwise the mutant would migrate as a dimer or oligomers on SDS-PAGE. To confirm this, we recorded the ^{15}N-^{1}H HSQC NMR spectrum of the mutant with near equimolar $HgCl_2$. This spectrum is significantly different from the spectrum of the $HgCl_2$ free sample, with many peak shifts and a large number of peaks either disappearing or diminishing in intensity (Supplementary Fig. 6a–c). This suggests the $HgCl_2$ cross-linking traps oxidized TtCcdA in a metastable state which shows a global difference from the ground outward-facing state. The cross-linking experiment demonstrates that the inward-facing state is accessible to oxidized TtCcdA.

Next, we wanted to ask whether the outward- and inward-facing conformational switch happens *in vivo*. Data for this is available in the form of previous studies of the solvent

accessibility of EcDsbD[14,15]. The residues of TM1 and TM4 of EcDsbD have been systematically mutated to cysteine and their reactivity with a membrane impermeable alkylating reagent measured in spheroplasts. The C-terminal halves of the two transport helices (TM1b and TM4b) are exposed to the aqueous environment while the N-terminal halves (TM1a and TM4a) are not (Fig. 3c). TtCcdA and EcDsbD have significant sequence homology (28% identity and 57% similarity). We sought to understand the EcDsbD solvent accessibility using the structural models of TtCcdA. For TtCcdA, TM1b is only solvent exposed in the inward-facing state while TM4b is only solvent exposed in the outward-facing state (Fig. 3a). Neither state matches the observed solvent accessibility of EcDsbD. But if the two states are accessed alternately, the solvent accessibility data can be explained satisfactorily. This suggests oxidized CcdA indeed exchanges between the two states *in vivo*.

The outward-facing structure and inward-facing model suggest that TtCcdA uses an elevator-type transport mechanism[26]. The “O” scaffold is immobile in the membrane while the A-helices use a rotation movement to transfer the disulfide bond ~12 Å along the direction of the membrane norm (Supplementary Video). This rotation movement minimizes the hydrophobic mismatch as the result of TM1 and TM4 moving in and out of the membrane and maximizes the vertical translation of the disulfide bond. The disulfide bond runs against the inside surface of TM3 and TM6, which is tightly packed and hydrophobic in the middle to prevent solvent leakage while loosely packed and hydrophilic at both ends to encourage water penetration, which is important for the thiol-disulfide exchange reactions between CcdA and its substrates (Fig. 4a).

The transport helices are loosely packed inside the “O” scaffold domain and the two parts are connected by flexible loops. An interesting question is what determines the up and down positions of the transport helices. Two conserved glycines, one eight residues preceding the first reactive cysteine (G12) and the other ten residues preceding the second reactive cysteine (G117), were found to be important to CcdA activity (Supplementary Fig. 4d)[12,13]. In TtCcdA, G12 belongs to a conserved Ax_3G motif on TM1a and G117 belongs to a conserved Ax_3Gx_3A motif on TM4a. In the outward-facing structure, the Ax_3G motif on TM1a packs against another conserved Ax_3G motif on TM5 (Fig. 4b). A pair of Ax_3G motifs and its variations are known to facilitate TM helix packing[27,28]. We mutated glycine G154 in the Ax_3G motif of TM5 to alanine. Such a small change in this tightly packed area results in severe destabilization of the outward-facing state, evidenced by the deteriorated NMR spectrum of this mutant (Supplementary Fig. 6d). In the inward-facing state, the Ax_3Gx_3A motif on TM4a packs against a conserved glycine, G49, on TM2. The alternate association and dissociation of these glycine-containing motifs may play a major role in the alternating-access of TtCcdA. The strengths of these interactions may be one of the major factors in determining the relative population of the inward and outward-facing states of TtCcdA.

Discussion

Transport mechanism of TtCcdA

We propose a multiple-step mechanism for the transport of reducing equivalents across the membrane by TtCcdA (Fig. 5). The outward-facing NMR structure likely represents the

ground state of oxidized TtCcdA. It is in a state in which TtCcdA has reduced the periplasmic substrates and forms an internal disulfide bond which remains at the periplasmic side of the protein. In this state, C127 is more exposed to the periplasm than C20, suggesting that the reactive cysteine on TM4 directly interacts with the periplasmic substrates. We have shown oxidized TtCcdA could convert to an inward-facing state in which the transport helices TM1 and TM4 carry the disulfide bond to the cytoplasmic side of the protein. The outward to inward conformational transition could be spontaneous or could be facilitated by interaction with cytoplasmic Trx. In the inward-facing model, C20 is more exposed to the cytoplasm than C127, suggesting the reactive cysteine on TM1 directly interacts with Trx. This is consistent with previous experimental observations[2].

Immediately after being reduced by the cytoplasmic Trx, TtCcdA would be in an inward-facing state in which both reactive cysteines remain at the cytoplasmic side. To reduce the periplasmic substrate, it is necessary for reduced TtCcdA to convert to an outward-facing state in which both reactive cysteines move to the periplasmic side. Without the internal disulfide bond, TM1 and TM4 could move independently, resulting in two potential intermediate states with one reactive cysteine at each side of the protein. The NMR spectrum of reduced TtCcdA suggests the reduced protein might exchange between multiple conformations (Fig. 1c). The tryptophan side chain NMR signals of the reduced-state mimic of AfCcdA also suggests that the reduced protein has multiple conformational states[23]. Further studies are needed to delineate the population and conformational exchange of the reduced states of CcdA.

The LysE superfamily of membrane transporters

From bioinformatics analysis (for example Pfam, http://pfam.xfam.org/clan/LysE), CcdA belongs to the LysE superfamily of membrane transporters. According to the Transporter Classification Database (TCDB, http://http://www.tcdb.org/superfamily.php?id=9), the LysE superfamily contains six families of divalent ion transporters, three families of amino acid transporters, one family of peptidoglycolipid transporter, and the CcdA family. Besides sequence homology, the internal 3-TM repeats are detected in several families of the LysE superfamily[29]. Bioinformatics analysis and mutagenesis studies found conserved and functionally important motifs locate on TM1 and TM4[29,30]. The sequence homology, the inverted 3-TM repeats, and the conserved motifs suggest that the members of the LysE superfamily may share a common fold. TtCcdA could serve as a template to model other LysE transporters and to better understand their mechanistic and functional attributes.

Membrane transporters using 3-TM repeats as building blocks

CcdA, semiSWEET, Pnu, and MFS transporters share the use of 3-TM repeats as their basic building blocks. semiSWEET sugar transporter is a parallel dimer of 3-TM bundles (Fig. 6a)[31]. The three helices of each bundle are connected in a right-handed order (Fig. 6e). Pnu vitamin transporters contain two parallel 3-TM repeats and a linker TM helix in between (3+1+3 TM, Fig. 6b)[32]. Each 3-TM bundle displays a linear arrangement of the three helices (Fig. 6f). A potential domain swapping evolutionary mechanism connecting the semiSWEET and Pnu transporters has been proposed[33]. Pnu and semiSWEET form an interesting contrast to CcdA that consists of two antiparallel left-handed 3-TM bundles (Fig.

6c and 6g). So far, Pnu and semiSWEET represent the minimal model of rocker-switch type transporters while CcdA is the smallest model of elevator transporters[26,31,34]. It will be interesting to see whether the 2 × 3-TM bundle represents the minimalist arrangement of natural membrane transporters. A non-natural designed zinc transporter with a 4 × 1-TM arrangement has been developed[35].

MFS is a large and diverse group of secondary transporters and facilitators which share the common architecture known as the MFS-fold[36]. MFS transporters consist of four left-handed 3-TM bundles (Fig. 6d and 6h)[37,38]. The N and C-terminal domains of MFS are pseudo-symmetrical and are parallel. Within each domain, the two pseudo-symmetrical and antiparallel 3-TM repeats show similar arrangement as in TtCcdA. Using the N-domain as an example, TM1 and TM4 are in the center of the domain and are inserted into the opposite 3-TM bundles. TM3 and TM6 pack against each other. A difference is that TM2 and TM5 are separated from each other and pack against TM11 and TM8, respectively, which are the C-domain counterparts of TM5 and TM2. To our knowledge, the 6-TM folds of CcdA and MFS domains are not observed in other membrane proteins.

Alternating access is a general framework to understand the mechanisms of membrane transporters. It posits that the substrate is alternately exposed to either side of the membrane through conformational changes of the membrane transporter[39]. Structural studies have revealed a spectrum of examples within this framework[26]. At one end, such as in the rocker-switch mechanism, the substrate-binding site is relatively immobile inside the membrane and the membrane transporter rearranges its conformation around this site. At the other end, such as in the elevator mechanism, the substrate-binding site is moved across the membrane via protein conformational change. semiSWEET uses an inter-3-TM-bundle rocker-switch movement to transport substrates[34]. MFS transporters use an inter-6-TM-domain rocker-switch movement to alternatively expose the substrates to both sides of the membrane[26,36,40]. CcdA relies on inter-6-TM-domain helix movement to shuttle the substrate to either side of the membrane. MFS and semiSWEET achieve similar transport mechanism using different combinations of different 3-TM bundles. MFS and CcdA provide an intriguing example that different transport mechanisms can be realized using a single or a combination of the same 6-TM fold.

Online Methods

TtCcdA expression and purification

The expression vector of TtCcdA was constructed by inserting an *E. coli* codon-optimized sequence (GenScript) encoding TtCcdA (GI 55981378) and a C-terminal "-PSHHHHHHHH" tag between the NdeI and XhoI sites of pET22b vector. An E35A mutation was introduced by site-directed mutagenesis to facilitate the expression of the full-length protein in *E. coli*. All other mutations were introduced on this background. BL21(DE3)pLysS competent cells were transformed and colonies from freshly transformed plates were used to inoculate 2.0 L LB medium. Cells were grow at 37 °C with vigorous shaking. When the optical density at 600 nm (OD_{600}) reached 0.7~0.8, cells were harvested by centrifugation, washed by 0.2 L M9 minimal medium, resuspended into 1.0 L M9 minimal medium supplemented with biotin (1 mg/L), thiamine (1 mg/L), and continue grow

at 37 °C. Cells were induced by 0.4 mM IPTG one hour after resuspension, harvested 1.5 hours after the induction, and lysed by three passes through an EmulsiFlex-C3 homogenizer (Avestin Inc.) in a buffer containing 50 mM Tris, pH 8.0, 300 mM NaCl, 0.02% sodium azide. Un-lysed cells were removed by centrifugation at 8,000g for 10 min. The membrane fraction was pelleted by ultracentrifugation at 100,000g for 1 hour and re-suspended into the above Tris buffer using a Dounce homogenizer. TtCcdA was extracted from the membrane by adding DDM to a final concentration of 1.5% (v/w). The membrane extraction proceeded at 4 °C overnight, during which time TtCcdA became fully oxidized. The DDM insoluble fraction was removed by a second ultracentrifugation. The DDM solubilized membrane protein was loaded onto a TALON column (Clontech Laboratory, Inc.). The column was washed with 20 column volumes the above Tris buffer containing DM (4.2 mM), DPC (1.5 mM), and 20 mM imidazole. TtCcdA was eluted by 4 column volumes of the above washing buffer plus 230 mM imidazole. To prepare NMR samples, 8.0 mL TtCcdA was concentrated to 0.2 mL by centrifugation using an Amicon Ultra-15 (MWCO 10kDa, Merck Millipore Inc.) centrifugal filter unit. Subsequently, TtCcdA was exchanged into NMR buffer (25 mM sodium acetate, 25 mM KH_2PO4, pH 5.4, 50 mM NaCl, 0.5 mM DPC, 10% D_2O) by 4 cycles of five-fold dilution and concentration. A typical TtCcdA NMR sample concentration was 0.25 mM.

[U-^{15}N]-TtCcdA and [U-^{2}H, ^{13}C, ^{15}N]-TtCcdA were expressed using ^{15}N and ^{2}H/^{13}C/^{15}N labeled M9 minimal media, respectively. Seven [U-^{15}N, ^{14}N-Xxx]-TtCcdA proteins were expressed using ^{15}N labeled M9 medium supplemented with ^{14}N labeled amino acids (0.15 g Ala to unlabel Ala, 0.5 g Arg to unlabel Arg, 0.15 g Cys to unlabel Cys, 0.5 g Gly to unlabel Gly and Ser, 1 g Leu to unlabel Leu, Ile, and Val, 0.5 g Lys to unlabel Lys, 1 g Phe to unlabel Phe and Tyr).

Thermus thermophilus Trx (TtTrx) expression and purification

The expression vector for TtTrx was constructed by inserting a synthetic DNA (GenScript) encoding TtTrx (TTHA1747) and an N-terminal “MGHHHHHHSSGENLYFQGS” tag between the NdeI and XhoI sites of pET22b vector. TtTrx was expressed using Rosetta(DE3) cells grown in M9 minimal medium supplemented with 1% (v/v) Bioexpress-1000 (Cambridge Isotope Laboratories). Cells were induced by 0.4 mM IPTG when OD_{600} reached 0.6 ~ 0.8. Expression continued for 6 hours at 30 °C and cells were harvested by centrifugation. TtTrx was purified using Ni-NTA chromatography, TEV protease cleavage, and a second Ni-NTA chromatography step to remove the affinity tag.

Activity assay

The reaction buffer contains 50 mM Tris, pH 8.0, 100 mM NaCl, 0.5 mM EDTA and was degassed before use. Purified oxidized TtCcdA was exchanged into the reaction buffer with 4.2 mM DM using a PD-10 column. Purified TtTrx was reduced by 10 mM DTT on ice for one hour and then exchanged into the reaction buffer using a PD-10 column. For the activity assay, 10 μM oxidized TtCcdA and 1.5% (w/v) DDM were mixed first and 50 μM freshly reduced TtTrx was added to trigger the reaction at 25 °C. At 20 sec, 1, 2, 4, 8, 16, 32, and 64 min time points, 10 μL of the reaction mixture was removed and mixed with 10 μL non-reducing SDS-PAGE loading buffer (contains 2% SDS). SDS quenches the reaction

effectively. Samples were then subjected to SDS-PAGE and Coomassie Brilliant Blue Staining.

Resonance assignments of TtCcdA

All NMR experiments were conducted at 70 °C on a Bruker AVANCE III 800 MHz spectrometer equipped with a cryogenic probe. NMR chemical shift assignments of backbone $^{1}H^{N}$, ^{15}N, ^{13}C, $13C^{\alpha}$ and side chain C^{β} were achieved using TROSY versions of HNCA, HN(CO)CA, HNCO, HN(CA)CO, and HN(CA)CB experiments. The assignments in the α-helical regions were confirmed by a 3D TROSY-based ^{15}N-edited NOESY-HSQC experiment. These experiments were performed on a [U-^{2}H, ^{13}C, ^{15}N]-TtCcdA sample. In addition, seven selectively counter labeled samples ([U-^{15}N, ^{14}N-Xxx]-TtCcdA) were used to facilitate the assignment (see the TtCcdA expression and purification section for the list of the seven samples).

PRE restraints

Nitroxide spin labels were introduced into the wild-type TtCcdA through single cysteine mutagenesis. Wild-type TtCcdA has two native cysteines, which form an internal disulfide bond during expression and purification. Eight mutation sites (L44C, F55C, V78C, L93C, A134C, F147C, F165C, and L186C) were used in the structure determination of oxidized TtCcdA. Purified TtCcdA mutants were labeled with two aliquots of a ten-fold excess of MTSL ((1-oxyl-2,2,5,5-tetramethyl-h3-pyrroline-3-methyl) methanethiosulfonate, Toronto Research Chemicals) at ambient temperature separated by one hour. Unreacted label was removed using a TALON column. Two TROSY-HSQC spectra for each mutant were recorded before and after the nitroxide label was reduced by five-fold excess of ascorbic acid. The native disulfide bond formation in these samples was checked by (1) the close resemblance of the diamagnetic NMR spectra of the mutants to that of the oxidized wild type protein and (2) the lack of a reduced protein band on SDS-PAGE. The completeness of the labeling was assessed by the total disappearance of certain peaks in the paramagnetic NMR spectra corresponding to residues in close proximity to the site of labeling. PRE distance restraints were derived from the intensity ratios of peaks in the paramagnetic and diamagnetic spectra (I_{para}/I_{dia})[17,19]. The global rotational correlation time of TtCcdA (30 ns) was determined using the [^{15}N,^{1}H]-TRACT experiment. The raw I_{para}/I_{dia} was calibrated using 10 residues unperturbed by the nitroxide spin labels (> 26 Å) to compensate for the concentration difference of the diamagnetic and paramagnetic samples. The I_{para}/I_{dia} was converted to PRE distance (r) using the following relationship: (1) I_{para}/I_{dia} <= 0.157, r = 0 ~ 17.2 Å, (2) 0.157 < I_{para}/I_{dia} <= 0.260, r = 13.8 ~ 18.2 Å, (3) 0.260 < I_{para}/I_{dia} <= 0.372, r = 15.1 ~ 19.3 Å, (4) 0.372 < I_{para}/I_{dia} <= 0.480, r = 16.2 ~ 20.6 Å, (5) 0.480 < I_{para}/I_{dia} <= 0.578, r = 17.1 ~ 21.8 Å, (6) 0.578 < I_{para}/I_{dia} <= 0.661, r = 17.9 ~ 23.3 Å, (7) 0.661 < I_{para}/I_{dia} <= 0.730, r = 17.7 ~ 25.1 Å, (8) 0.730 < I_{para}/I_{dia} <= 0.785, r = 19.6 ~ 26.7 Å, (9) 0.785 < I_{para}/I_{dia} <= 0.800, r = 20.2 ~ 27.4 Å, (10) 0.800 < I_{para}/I_{dia}, r = 20.4 ~ 200 Å. In deriving the above relationship, two sources of errors were considered: the error in peak intensities and the error of R_2 estimation of the diamagnetic samples. In the structure calculation, the paramagnetic labels are treated as floating points restrained to be within 6 Å from the Cβ atoms of the corresponding mutated residues. The PRE distance restraints were used in the

same manner as the NOE distance restraints except the force constant was 1/25 of the latter one, which reflects its larger error.

RDC restraints

Two independent alignments were induced using a positively charged compressed gel and a neutral stretched gel. The positively charged gel was composed of 2.0 % (w/v, final concentration) acrylamide and 2.0 % (w/v, final concentration) (3-acrylamidopropyl)-trimethylammonium chloride (APTMAC) and was vertically compressed from 21 mm to 16 mm in a Shigemi NMR tube, as described previously[18]. The 3.8% (w/v) neutral acrylamide gel was stretched from 6.0 mm diameter to 4.24 mm diameter inside an open end NMR tube. Both gels withstood the high temperature measurements without significant shrinking. ^{15}N-^{1}H RDC was recorded using the ARTSY experiment on perdeuterated samples[20]. The error of the RDC restraints was estimated by the noise of the spectra and a minimal error of ±2.5 Hz was imposed. The initial alignment amplitudes and rhombicities were estimated by powder pattern analysis and were allowed to change during structure calculations.

Structure calculation

The structures were calculated using XPLOR-NIH. A two-step folding and refinement protocol was used. In the folding step, initial structures were folded from an extended conformation using dihedral angle restraints, short-range NOE restraints, hydrogen bond restraints, and PRE restraints. The backbone ϕ and φ dihedral angle restraints were derived from the chemical shifts using TALOS-N[41]. The errors were set using TALOS-N default values: 20 degrees or 2 times the TALOSN derived standard deviation, whichever is larger, for strong predictions; 30 degree or 3 times the TALOSN derived standard deviation, whichever is larger, for generous predictions. The short-range NOE restraints were derived from a 3D ^{15}N-edited NOESY-TROSY experiment and were only observed between i and i +1, i+2 backbone amides. Residues for which hydrogen bond restraints were used were identified using a D/H exchange experiment. For residues that resist D/H exchange and are in the TALOS-N predicted α-helical regions, standard XPLOR-NIH α-helical backbone hydrogen bond restraints were imposed. Structures were calculated using ~100 ps of torsion angle dynamics at 3500 K followed by ~260 ps of slow cooling in torsion angle space. In total, 200 structures were calculated and the 10 structures of lowest energy were subject to further refinement (Supplementary Fig. 2d). In the refinement step, RDC restraints and an implicit membrane potential were used[42]. Structures were calculated using 40 ps of torsion angle dynamics at 3000 K followed by ~160 ps of slow cooling in torsion angle space. In total, 200 structures were calculated and the 10 structures of lowest energy were chosen to represent the ensemble structure of TtCcdA. From this ensemble, the lowest energy structure is used as the representative structure. Molprobity reported 95% of all residues were in favored regions and 99% of all residues were in allowed regions of the Ramachandran plot.

Structure validation

To assess the robustness of the TtCcdA structure, we have repeated the structure calculation using reduced numbers of the long-range PRE and/or RDC restraints: (1) PREx6 using PRE restraints from six samples (L44C, V78C, A134C, F147C, F165C, and L186C), (2) PREx7 using PRE restraints from L93C sample in addition to the restraints used in PREx6, (3)

PREx8 using all PRE restraints, and (4) PREx8+RDCx1 using all PRE restraints plus RDC restraints from the positively charged sample. In each structure calculation, the 10 structures of lowest energy were chosen to represent the structure ensemble. They were compared with the representative structure and the average r.m.s.d. was reported (Supplementary Fig. 2e). They were also checked against the withheld data from the neutral gel and the average Q_{free} was reported. When all RDC restraints and one set of the PRE restraints were removed (PREx7, ~30% long range structural restraints removed), the calculated structures still resemble the reported structure.

Solvent accessibility of TtCcdA

Solvent accessibility of TtCcdA was measured by a titration experiment with Gd-DTPA (Diethylenetriaminepentaacetic acid gadolinium). Gd-DTPA was dissolved at 200 mM in NMR buffer and the buffer pH was readjusted. Two TtCcdA samples with and without 20 mM Gd-DTPA were prepared and TROSY-HSQC spectra were recorded. The PRE effects were defined as the signal intensity ratio of the paramagnetic spectrum to the reference spectrum.

Model building of inward-facing TtCcdA

We followed an established repeat-swap homology modeling protocol to construct the inward-facing model of oxidized TtCcdA [24]. The structural repeating units are TM1–3 (residues 4~91) and TM4–6 (residues 109~199). Their sequence alignment was generated using T-coffee. The initial alignment was further adjusted by shifting the TM1a by −1 residue. The full-length alignment of the model and the template was constructed by joining the TM1–3 and TM4–6 fragment alignment (Supplementary Fig. 5a–b). The non-repeating membrane peripheral elements (residues 92–94, 200–222) were aligned to themselves. The flexible loops (residues 1–3, 32–39, 95–108, 141–145) were not aligned and their conformations were generated *de novo*. To conserve the secondary structure of the template, both ends of TM1 and TM4, and N-terminal of TM2 and TM5 were constrained to be α-helical. To conserve the conformation of the “O” scaffold and H1 helix, distance restraints between Cα atoms were introduced in these regions (residues 50–91, 155–199, and 207–214). The inward-facing model was built using MODELLER (version 9.17). A total of 200 models were calculated and a representative model was chosen based on low molPDF and DOPE scores.

Cysteine cross-linking experiment

The purified TtCcdA was exchanged into the degassed cross-linking reaction buffer (the activity buffer without EDTA) using a PD-10 column. To induce cross-linking, 20 μM protein was mixed with 22 μM $HgCl_2$ and the sample was incubated on ice for 15 minutes. To label the free cysteines, the sample was mixed with 2.0 mM 5 kDa PEG maleimide (malPEG5K) and the reaction was kept at room temperature for 30 minutes. The reaction products were separated using non-reducing SDS-PAGE (4~20% gradient gel).

Data Availability

The accession number for the coordinates and structural restraints of TtCcdA is PDB: 5VKV and BMRB: 30286. The PMDB accession code for the inward-facing model of TtCcdA is PM0081003. A Life Sciences Reporting Summary for this article is available.

Supplementary Material

Refer to Web version on PubMed Central for supplementary material.

Acknowledgments

We thank J. F. Ellena for support and advice on NMR. We thank D. S. Cafiso for scientific discussions. This work was supported by grant R01GM078296 to J.H.B. from the National Institutes of Health.

References

1. Stewart EJ, Katzen F, Beckwith J. Six conserved cysteines of the membrane protein DsbD are required for the transfer of electrons from the cytoplasm to the periplasm of Escherichia coli. EMBO J. 1999; 18:5963–5971. [PubMed: 10545108]
2. Katzen F, Beckwith J. Transmembrane electron transfer by the membrane protein DsbD occurs via a disulfide bond cascade. Cell. 2000; 103:769–779. [PubMed: 11114333]
3. Collet JF, Riemer J, Bader MW, Bardwell JCA. Reconstitution of a disulfide isomerization system. J Biol Chem. 2002; 277:26886–26892. [PubMed: 12004064]
4. Malojčić G, Geertsma ER, Brozzo MS, Glockshuber R. Mechanism of the prokaryotic transmembrane disulfide reduction pathway and its in vitro reconstitution from purified components. Angew Chemie - Int Ed. 2012; 51:6900–6903.
5. Katzen F, Deshmukh M, Daldal F, Beckwith J. Evolutionary domain fusion expanded the substrate specificity of the transmembrane electron transporter DsbD. EMBO J. 2002; 21:3960–3969. [PubMed: 12145197]
6. Cho SH, et al. A new family of membrane electron transporters and its substrates, including a new cell envelope peroxiredoxin, reveal a broadened reductive capacity of the oxidative bacterial cell envelope. MBio. 2012; 3:1–11.
7. Cho SH, Collet JF. Many Roles of the Bacterial Envelope Reducing Pathways. Antioxid Redox Signal. 2013; 18:1690–1698. [PubMed: 23025488]
8. Simon J, Hederstedt L. Composition and function of cytochrome c biogenesis System II. FEBS J. 2011; 278:4179–4188. [PubMed: 21955752]
9. Bardischewsky F, Fischer J, Höller B, Friedrich CG. SoxV transfers electrons to the periplasm of Paracoccus pantotrophus - An essential reaction for ohemotrophic sulfur oxidation. Microbiology. 2006; 152:465–472. [PubMed: 16436434]
10. Page MLD, et al. A homolog of prokaryotic thiol disulfide transporter CcdA is required for the assembly of the cytochrome b6f complex in Arabidopsis chloroplasts. J Biol Chem. 2004; 279:32474–32482. [PubMed: 15159384]
11. RAK, Martin L, Saier MHJ. Reversing transmembrane electron flow: the DsbD and DsbB protein families. J Mol Microbiol Biotechnol. 2003; 5:133–149. [PubMed: 12766342]
12. Cho SH, Beckwith J. Mutations of the membrane-bound disulfide reductase DsbD that block electron transfer steps from cytoplasm to periplasm in Escherichia coli. J Bacteriol. 2006; 188:5066–5076. [PubMed: 16816179]
13. Hiniker A, Vertommen D, Bardwell JCA, Collet JF. Evidence for conformational changes within DsbD: Possible role for membrane-embedded proline residues. J Bacteriol. 2006; 188:7317–7320. [PubMed: 17015672]
14. Cho SH, Porat A, Ye J, Beckwith J. Redox-active cysteines of a membrane electron transporter DsbD show dual compartment accessibility. EMBO J. 2007; 26:3509–3520. [PubMed: 17641688]

15. Cho SH, Beckwith J. Two Snapshots of Electron Transport across the Membrane: INSIGHTS INTO THE STRUCTURE AND FUNCTION OF DsbD. J Biol Chem. 2009; 284:11416–11424. [PubMed: 19258316]
16. Rozhkova A, Glockshuber R. Thermodynamic Aspects of DsbD-Mediated Electron Transport. J Mol Biol. 2008; 380:783–788. [PubMed: 18571669]
17. Zhou Y, et al. NMR Solution Structure of the Integral Membrane Enzyme DsbB: Functional Insights into DsbB-Catalyzed Disulfide Bond Formation. Mol Cell. 2008; 31:896–908. [PubMed: 18922471]
18. Cierpicki T, Bushweller JH. Charged gels as orienting media for measurement of residual dipolar couplings in soluble and integral membrane proteins. J Am Chem Soc. 2004; 126:16259–16266. [PubMed: 15584763]
19. Liang B, Bushweller JH, Tamm LK. Site-directed parallel spin-labeling and paramagnetic relaxation enhancement in structure determination of membrane proteins by solution NMR spectroscopy. J Am Chem Soc. 2006; 128:4389–4397. [PubMed: 16569016]
20. Fitzkee NC, Bax A. Facile measurement of 1H-15N residual dipolar couplings in larger perdeuterated proteins. J Biomol NMR. 2010; 48:65–70. [PubMed: 20694505]
21. Lomize MA, Pogozheva ID, Joo H, Mosberg HI, Lomize AL. OPM database and PPM web server: Resources for positioning of proteins in membranes. Nucleic Acids Res. 2012; 40:370–376.
22. Deshmukh M, Brasseur G, Daldal F. Novel Rhodobacter capsulatus genes required for the biogenesis of various c-type cytochromes. Mol Microbiol. 2000; 35:123–138. [PubMed: 10632883]
23. Williamson JA, et al. Structure and multistate function of the transmembrane electron transporter CcdA. Nat Struct Mol Biol. 2015; 22:809–814. [PubMed: 26389738]
24. Vergara-Jaque A, Fenollar-Ferrer C, Kaufmann D, Forrest LR. Repeat-swap homology modeling of secondary active transporters: Updated protocol and prediction of elevator-type mechanisms. Front Pharmacol. 2015; 6:1–12. [PubMed: 25805991]
25. Mulligan C, et al. The bacterial dicarboxylate transporter VcINDY uses a two-domain elevator-type mechanism. Nat Struct Mol Biol. 2016; 23:256–263. [PubMed: 26828963]
26. Drew D, Boudker O. Shared Molecular Mechanisms of Membrane Transporters. Annu Rev Biochem. 2016; 85:543–572. [PubMed: 27023848]
27. Senes A, Engel DE, Degrado WF. Folding of helical membrane proteins: The role of polar, GxxxG-like and proline motifs. Curr Opin Struct Biol. 2004; 14:465–479. [PubMed: 15313242]
28. Mackenzie KR, Prestegard JH, Engelman DM. Implications A Transmembrane Helix Dimer: Structure and Implications. Science (80-). 1997; 276:131–133.
29. Tsu BV, Saier MH. The LysE superfamily of transport proteins involved in cell physiology and pathogenesis. PLoS One. 2015; 10
30. Colinet AS, et al. Acidic and uncharged polar residues in the consensus motifs of the yeast Ca2+ transporter Gdt1p are required for calcium transport. Cell Microbiol. 2017; 19
31. Xu Y, et al. Structures of bacterial homologues of SWEET transporters in two distinct conformations. Nature. 2014; 515:448–452. [PubMed: 25186729]
32. Jaehme M, Guskov A, Slotboom DJ. Crystal structure of the vitamin B 3 transporter PnuC, a full-length SWEET homolog. Nat Struct Mol Biol. 2014; 21:1013–1015. [PubMed: 25291599]
33. Jaehme M, Guskov A, Slotboom DJ. The twisted relation between Pnu and SWEET transporters. Trends Biochem Sci. 2015; 40:183–188. [PubMed: 25757400]
34. Lee Y, Nishizawa T, Yamashita K, Ishitani R, Nureki O. Structural basis for the facilitative diffusion mechanism by SemiSWEET transporter. Nat Commun. 2015; 6:6112. [PubMed: 25598322]
35. Joh NH, et al. De novo design of a transmembrane Zn2+-transporting four-helix bundle. Science (80-). 2014; 346:1520–1524.
36. Law CJ, Maloney PC, Wang DN. Ins and Outs of Major Facilitator Superfamily Antiporters. Annu Rev Microbiol. 2008; 62:289–305. [PubMed: 18537473]
37. Abramson J, et al. Structure and mechanism of the lactose permease of Escherichia coli. Science (80-). 2003; 301:610–615.

38. Yan N. Structural advances for the major facilitator superfamily (MFS) transporters. Trends Biochem Sci. 2013; 38:151–159. [PubMed: 23403214]

39. Jardetzky O. Simple allosteric model for membrane pumps. Nature. 1966; 211:969–970. [PubMed: 5968307]

40. Yan N. Structural Biology of the Major Facilitator Superfamily Transporters. Annu Rev Biophys. 2015; 44:257–283. [PubMed: 26098515]

41. Shen Y, Bax A. Protein backbone and sidechain torsion angles predicted from NMR chemical shifts using artificial neural networks. J Biomol NMR. 2013; 56:227–241. [PubMed: 23728592]

42. Tian Y, Schwieters CD, Opella SJ, Marassi FM. A Practical Implicit Membrane Potential for NMR Structure Calculations of Membrane Proteins. Biophys J. 2015; 109:574–585. [PubMed: 26244739]

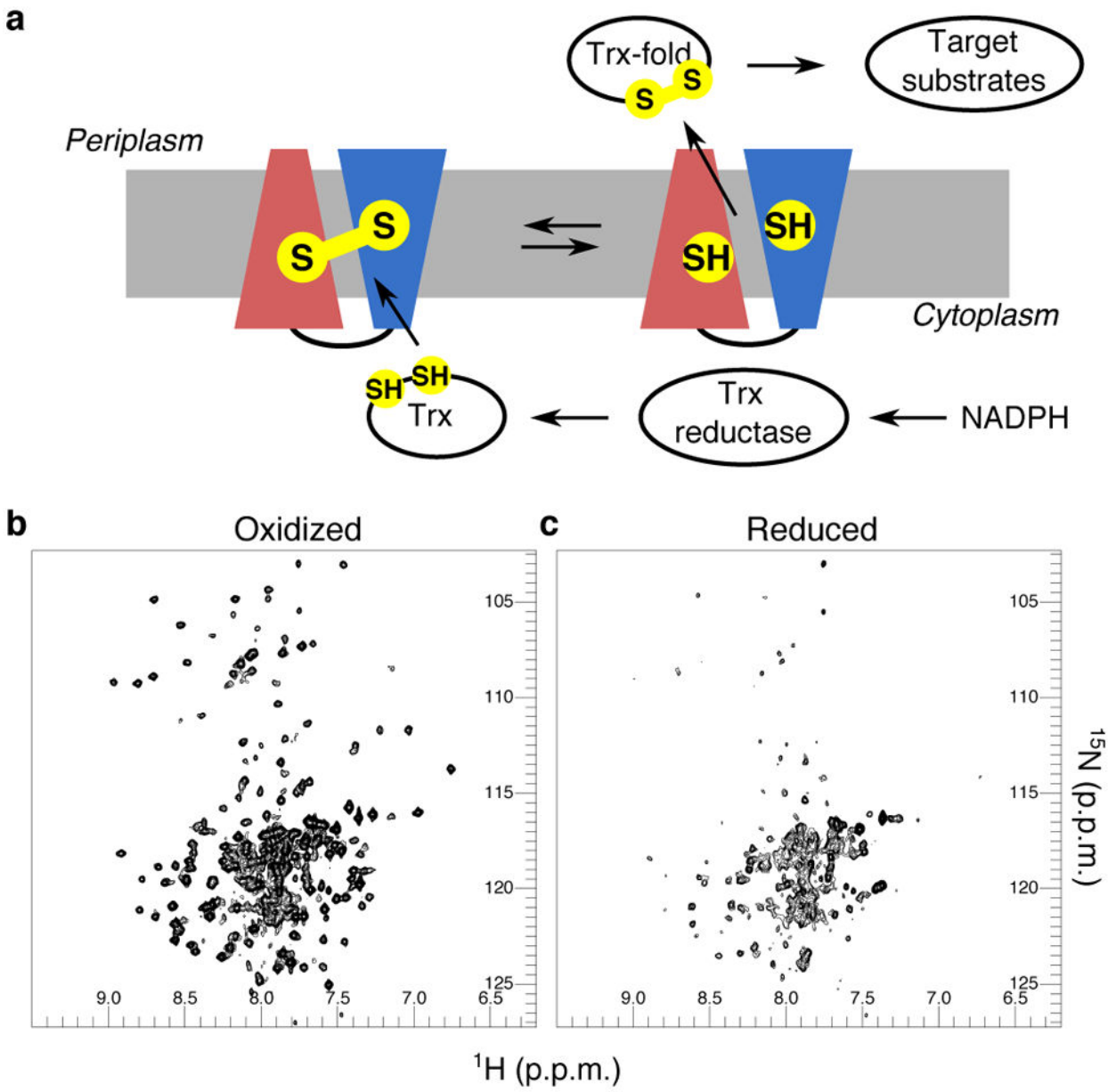

Figure 1.

CcdA reducing pathway and NMR spectra of TtCcdA. (a) Schematic of the CcdA reducing pathway. The two inverted 3-TM repeats are represented by red and blue trapezoids. (b) The [^{1}H,^{15}N]-TROSY-HSQC spectra of oxidized TtCcdA, recorded at 70°C and 800 MHz. (c) The [^{1}H,^{15}N]-TROSY-HSQC spectra of reduced TtCcdA (5 mM DTT), recorded under the same conditions.

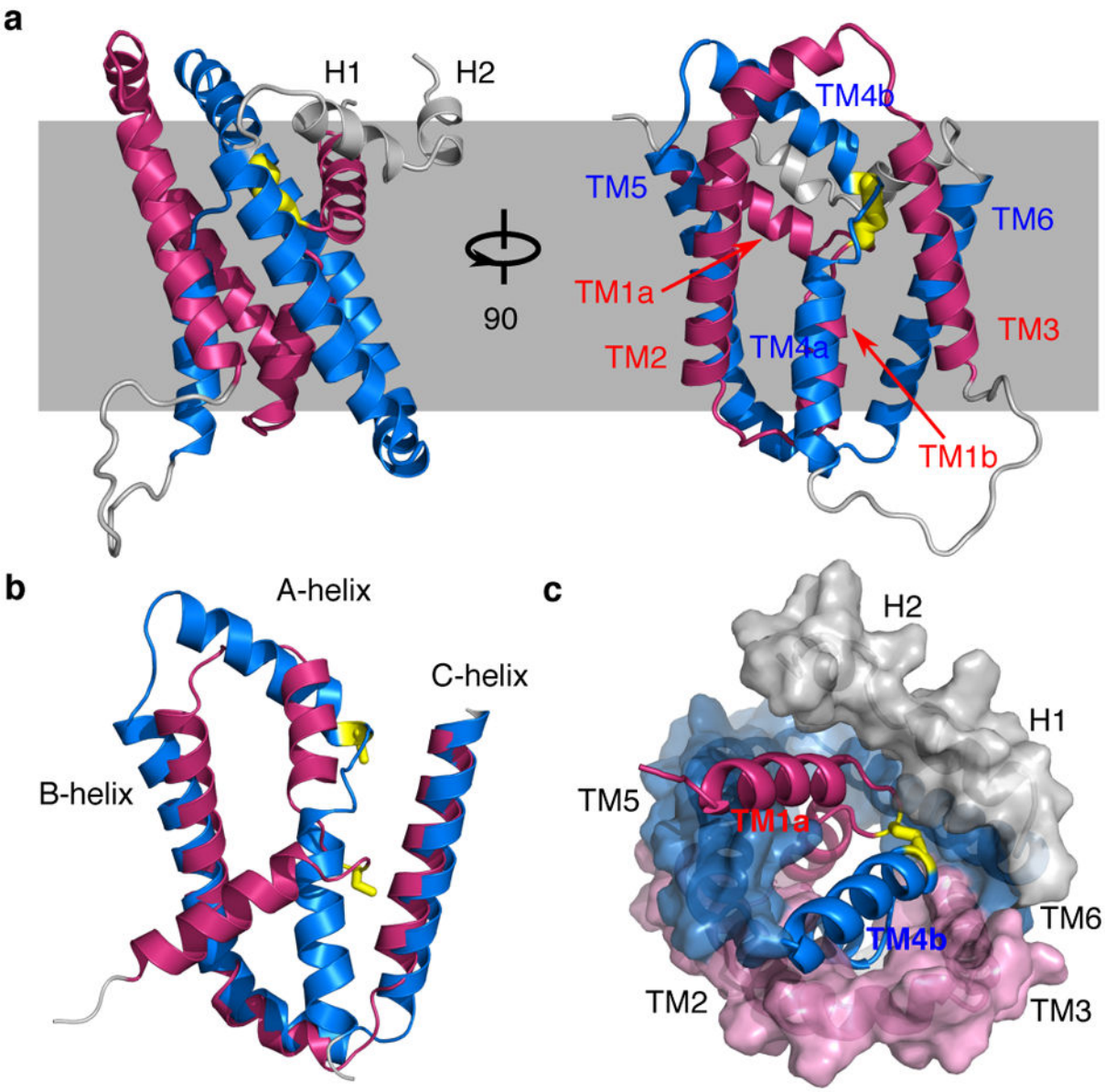

Figure 2.

Structure of oxidized TtCcdA. (a) Structure of oxidized TtCcdA viewed in the membrane. The disulfide bond is shown as yellow sticks. (b) Overlay of the two 3-TM bundles by the B and C-helices. (c) Cartoon representation of the transport helices and surface representation of the "O" scaffold, viewed from the periplasm.

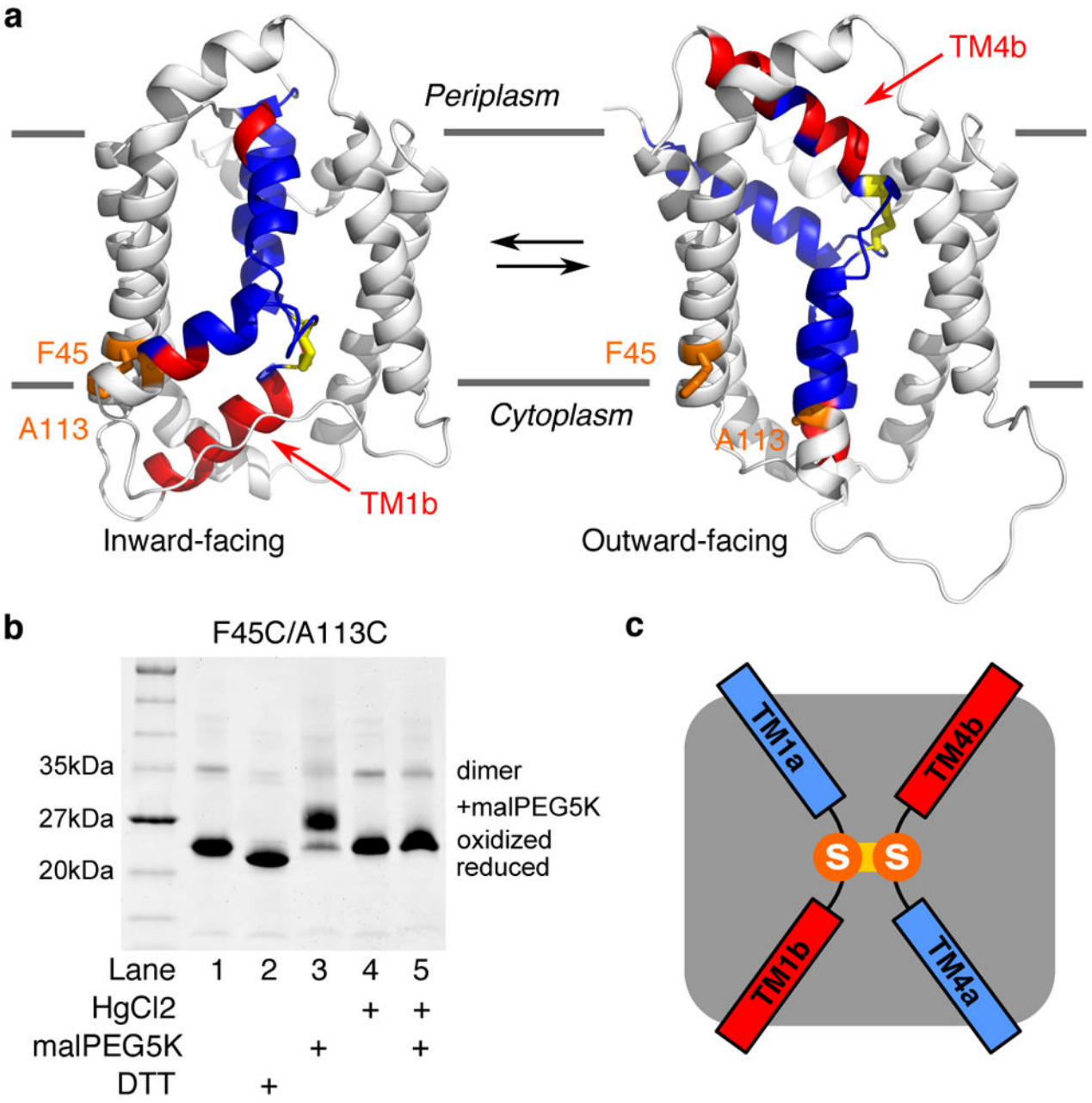

Figure 3.

Inward-facing model of oxidized TtCcdA. (a) Cartoon representation of the inward-facing model (left) and the outward-facing structure (right) of TtCcdA viewed in the membrane. The "O" scaffold is white. The A-helices are colored by their solvent accessible (red) and inaccessible (blue) portions. The cross-linking residues are orange. (b) SDS-PAGE showing the alkylation of the F45C/A113C mutant by malPEG5K with (+) and without (-) the protection of $HgCl_2$. The uncropped gel image is shown in Supplementary Data Set 1. (c) Schematic of the experimentally determined solvent accessible (red) and inaccessible (blue) regions of the A-helices of EcDsbD[14,15].

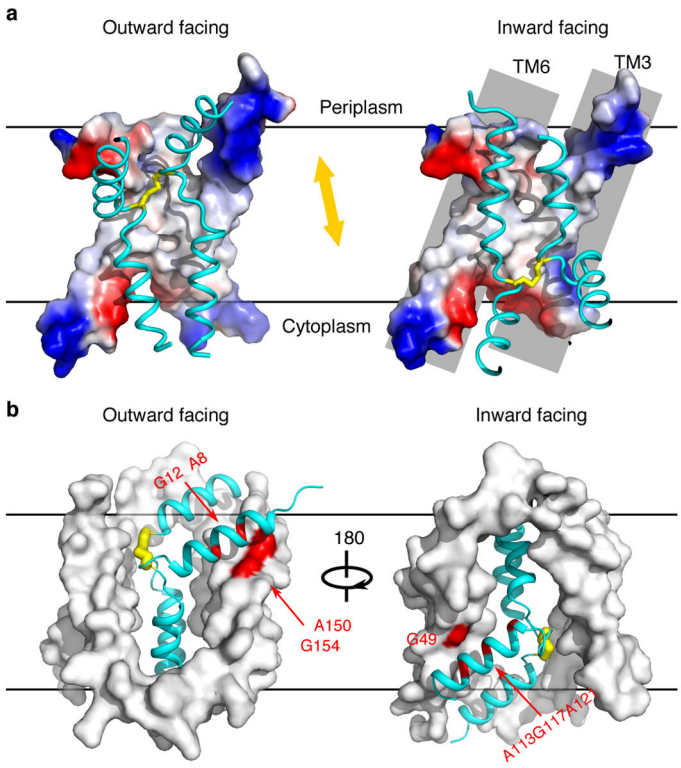

Figure 4.

Elevator-type movement of the transport helices. (a) Cartoon representation of the transport helices (cyan) and surface representation of the barrier helices viewed in the membrane plane from the direction of TM2 and TM5, which are removed for a clearer view. The disulfide bond is shown as yellow sticks and the orange arrow indicates the direction of its movement. The middle section of TM3 and TM6 is tightly packed via the Gx_6G motifs and is hydrophobic (white). Toward the periplasmic and cytoplasmic ends, the packing is loose and there are positively (blue) and negatively (red) charged residues. (b) The transport helices (cyan cartoon) move across the "O" scaffold domain (white surface) during transport. In the outward-facing state (left), the conserved Ax_3G motifs on TM1a and TM5 form a stable contact. In the inward-facing state (right), the conserved G49 on TM2 and Ax_3Gx_3A motif on TM4a associate at a symmetrical position.

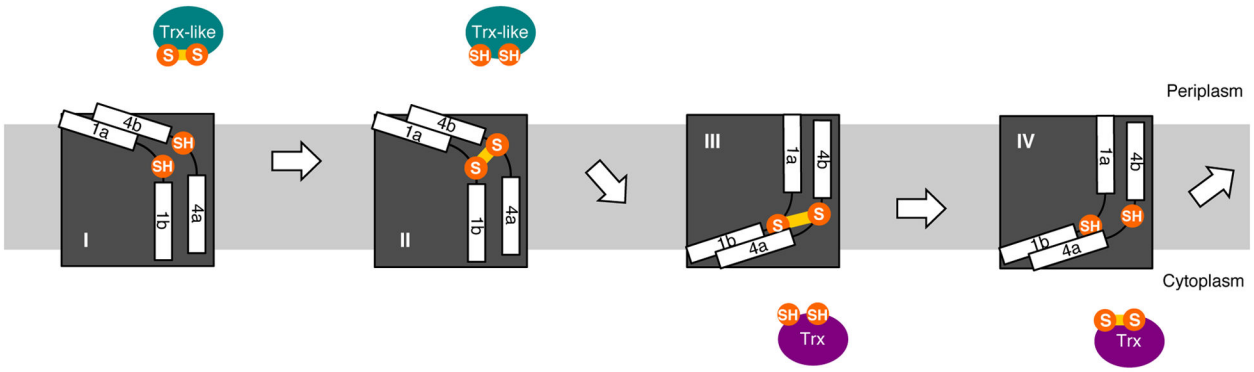

Figure 5.

Proposed reducing equivalent transport mechanism of CcdA. CcdA exchanges among four major conformational states during the transport cycle: (I) outward-facing reduced state, (II) outward-facing oxidized state, (III) inward-facing oxidized state, and (IV) inward-facing reduced state. The dark grey and the white boxes represent the “O” frame and the transport helices of CcdA, respectively. The disulfide bonds are shown as thick yellow line.

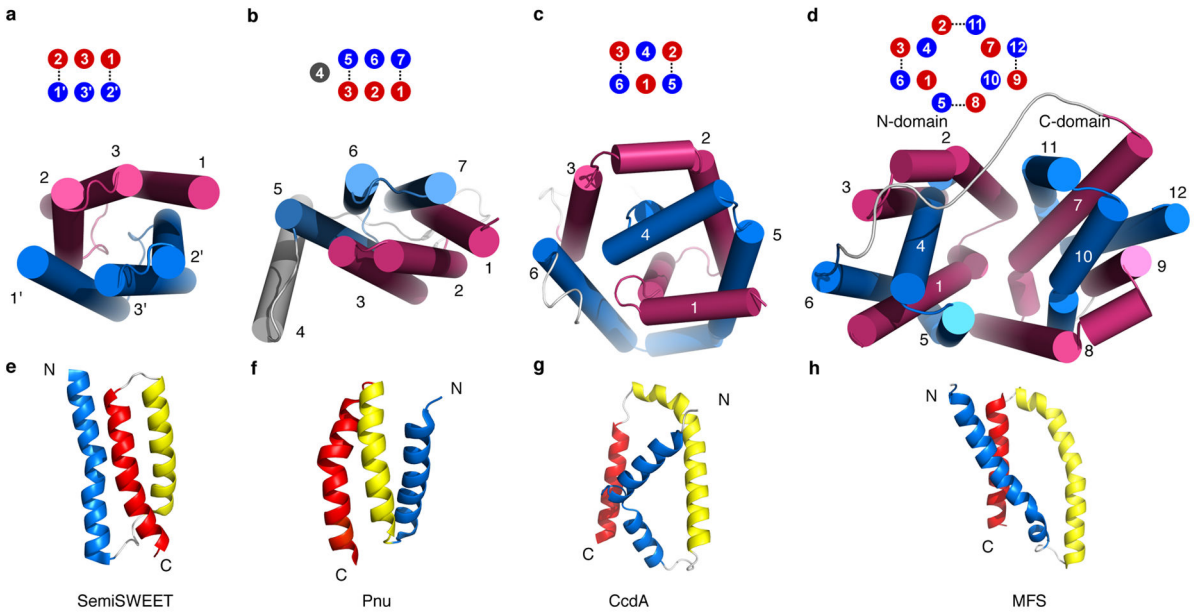

Figure 6.

Structural comparison of CcdA, semiSWEET, Pnu, and MFS. (a–d) Cartoon representations of the structures of semiSWEET (4QNC), Pnu (4QTN), TtCcdA, and MFS (1PV7). Neighboring 3-TM bundles are colored as red and blue. (e–h) Ribbon representations of the 3-TM bundles of semiSWEET, TtCcdA, Pnu, and MFS. The first, second, and third TM helices of each 3-TM bundle are colored blue, yellow, and red, respectively.

Table 1

NMR and Refinement Statistics for the TtCcdA Structure

	Protein
NMR distance and dihedral constraints	
Distance constraints	
short range NH-NH NOEs	151
Hydrogen bonds	56
PRE restraints	
upper bound	301
lower bound	895
Total dihedral angle restraints	
phi	185
psi	185
RDC restraints	
neutral gel	107
positively charged gel	100
Structure statistics	
Violations (mean and s.d.)	
Distance constraints (Å)	
Short range NOEs	0.0007 ± 0.0016
PREs	0.119 ± 0.006
Dihedral angle constraints (°)	0.11 ± 0.03
Max. dihedral angle violation (°)	0.153
Max. distance constraint violation (Å)	
Short range NOEs	0.005
PREs	0.127(1.396)
Deviations from idealized geometry	
Bond lengths (Å)	0.002 ± 0.000
Bond angles (°)	0.342 ± 0.003
Impropers (°)	0.295 ± 0.008
Average pairwise r.m.s.d.[a] (Å)	
Heavy	2.9
Backbone	1.9

[a]Statistics are calculated over an ensemble of 10 lowest energy structures from the 200 structures calculated and are applied in helical and rigid loop regions (residues 4–32, 39–94, 110–139, 146–220).